Computing solubility parameters of deep eutectic solvents from Molecular Dynamics simulations

Seyed Salehi, Hirad; Ramdin, Mahinder; Moultos, Othonas A.; Vlugt, Thijs J.H.

DOI
10.1016/j.fluid.2019.05.022

Publication date
2019

Document Version
Accepted author manuscript

Published in
Fluid Phase Equilibria

Citation (APA)
Seyed Salehi, H., Ramdin, M., Moultos, O. A., & Vlugt, T. J. H. (2019). Computing solubility parameters of deep eutectic solvents from Molecular Dynamics simulations. *Fluid Phase Equilibria*, *497*, 10-18. https://doi.org/10.1016/j.fluid.2019.05.022

Computing solubility parameters of Deep Eutectic Solvents from Molecular Dynamics simulations

Hirad S. Salehi[a], Mahinder Ramdin[a], Othonas A. Moultos[a], Thijs J.H. Vlugt[a,*]

[a]*Engineering Thermodynamics, Process & Energy Department, Faculty of Mechanical, Maritime and Materials Engineering, Delft University of Technology, Leeghwaterstraat 39, 2628CB Delft, The Netherlands*

Abstract

The solubility parameter (SP) of a solvent is a key property that measures the polarity and quantifies the 'like-dissolves-like' principle, which is an important rule in chemistry for screening solvents for separation processes. It is challenging to experimentally obtain solubility parameters of non-volatile solvents like ionic liquids (ILs), deep eutectic solvents (DESs), and polymers. Here, Molecular Dynamics (MD) simulations have been used to compute the Hildebrand and Hansen solubility parameters of DESs, which are green solvents with potential applications in many different fields. The results from MD simulations are compared with limited available experimental data and commonly used SP correlations for non-volatile solvents. Very limited information is available in literature for the vapor phase composition of DESs. Solubility parameters are computed based on the vaporization of hydrogen bond donor (HBD) and hydrogen bond acceptor (HBA) components of the DESs as well as clusters, consisting of HBD and HBA components. The relatively large SPs computed from MD indicate that the investigated choline chloride-based DESs are polar solvents. The values of SPs are not significantly affected by temperature. A comparison of vaporization enthalpies of HBD, HBA and clusters from the DES mixture suggests that it is more likely for HBD molecules to vaporize from the DES mixture and dominate the vapor phase.

Keywords:
Solubility parameters, deep eutectic solvents, Molecular Dynamics simulation, polarity, vaporization enthalpy

1. Introduction

The polarity of a solvent is a key property for determining the ability of the solvent to dissolve various solutes, which is often discussed in the context of the 'like-dissolves-like' principle [1, 2]. In practice, the difficulty with using this principle lies in the fact that it

*Corresponding author
Email address: t.j.h.vlugt@tudelft.nl (Thijs J.H. Vlugt)

requires a method to quantify 'like' and 'unlike' or polar and non-polar compounds. The first attempt to quantify the 'like-dissolves-like' principle was made in 1936 by Hildebrand, who introduced the concept of solubility parameters (SPs) [3]. The Hildebrand solubility parameter, δ, is defined as the square root of the cohesive energy density (CED):

$$\delta = \sqrt{\frac{\Delta E_{\text{vap}}}{V_m}} \tag{1}$$

where ΔE_{vap} is the energy of vaporization and V_m the molar volume of the solvent.

Based on the vapor pressure data of a compound, the enthalpy of vaporization (ΔH_{vap}) can be computed by linear regression using the Clausius-Clapeyron relation [4]:

$$\frac{\mathrm{d}\ln P}{\mathrm{d}(1/T)} = -\frac{\Delta H_{\text{vap}}}{R} \tag{2}$$

where P and T are the coexistence pressure and temperature, respectively, and R is the universal gas constant. Assuming the gas phase is ideal gas, the vaporization energy can be computed using $\Delta E_{\text{vap}} = \Delta H_{\text{vap}} - RT$.

Although Equation (1) is simple to apply, it can only be used for non-polar and slightly polar compounds without specific interactions like hydrogen bonding. In addition, a complication may arise for non-volatile solvents like ionic liquids (ILs), deep eutectic solvents (DESs), and polymers due to the lack of experimental vapor pressure data, needed to obtain values for ΔE_{vap}. To overcome this limitation, the Hildebrand SP has been correlated with other physical quantities like surface tension, intrinsic viscosity, dielectric constants, melting points, activation energy of viscosity, infinite dilution activity coefficients from inverse gas chromatography, and group-contribution methods [5–18]. For instance, the SP is correlated with the surface tension,γ, as [15]:

$$\delta^2 = k\gamma V_m^{-1/3} \tag{3}$$

where V_m is the molar volume of the solvent and k is a constant that depends on the coordination number of molecules [15, 19]. Kilaru et al. [6] used Equation (3) to estimate SPs of ionic liquids. The intrinsic viscosity, η, is related to the SP through the Mangaraj equation [20]:

$$\eta = \eta_{\max} \exp(-A(\delta_{\text{solv}} - \delta_{\text{sol}})) \tag{4}$$

where A is a fitting parameter, δ_{solv} and δ_{sol} are the solubility parameters of the solvent and the solute, respectively. The intrinsic viscosity exhibits a maximum ($\eta_{\max}$) at a point where the mutual interaction between the solute and the solvent is the highest. The intrinsic viscosity method has been used to predict the SPs of ILs and polymers [8, 11, 20].

Moganty and Baltus [10] correlated the activation energy of viscosity ($E_{\text{a}}^{\text{vis}}$) with the SP of ILs as:

$$\delta = \sqrt{\frac{cE_{\text{a}}^{\text{vis}}}{V_m}} \tag{5}$$

in which c is a constant. The value of c largely depends on the shape and size of the molecule under consideration. For instance, c is set to 4 for non-spherical molecules and to 3 for small spherical molecules [21, 22]. The activation energy of viscosity appears explicitly in the Arrhenius-type equation, which is often used to model the temperature dependence of viscosity. However, some substances (e.g. molten salts with glass transition at low temperatures [23]) exhibit a non-Arrhenius behavior. For many ILs and DESs, the Vogel-Fulcher-Tammann (VFT) equation has been used to describe the temperature dependence of viscosity more accurately than the Arrhenius model [23–28]:

$$\eta = A \exp \frac{B}{T - T_0} \tag{6}$$

in which A, B and T_0 are constants, η is the viscosity and T the temperature. The temperature dependent activation energies, $E_{\mathrm{a}}^{\mathrm{vis}}(T)$, from the VFT equation are then computed by [29]:

$$E_{\mathrm{a}}^{\mathrm{vis}}(T) = BR \left(\frac{T}{T - T_0} \right)^2 \tag{7}$$

where T is the temperature, R is the universal gas constant, and B and T_0 are the constants in Equation (6) obtained by regression.

In 1967, Hansen extended the work of Hildebrand and introduced a solubility parameter, which accounts for the contributions from various interactions [30]:

$$\delta^2 = \delta_d^2 + \delta_p^2 + \delta_h^2 \tag{8}$$

where δ_d, δ_p, and δ_h, are contributions from dispersion (van der Waals) interactions, polar (dipole-dipole) interactions, and hydrogen bonding. The dispersion contribution is expected to be significant for non-polar solvents, whereas the polar component is larger for molecules with larger dipole moments. The hydrogen bonding term is used when hydrogen bonds exist between molecules in the system. In this case, dipole-dipole and dispersion forces are not sufficient to describe the overall polarity of molecules. Compounds with similar Hansen solubility parameters are miscible in most proportions, while dissimilar values yield partial miscibility or immiscibility [31, 32]. Therefore, knowledge of these solubility parameters can help in selecting solvents for certain applications. However, it is experimentally challenging to measure the polarity or (Hansen) solubility parameters, especially for non-volatile solvents. The ability of solvents to dissolve solutes is often experimentally measured by means of solvatochromic parameters, which are correlated with the hypsochromic (blue) or bathochromic (red) shift of the UV-vis spectra of certain probe molecules (dyes) as a function of the solvent polarity [33, 34]. The two most commonly used polarity scales are the Reichardt's dye scale (E_{T} parameter) [35, 36] and the Kamlet-Taft (KT) scale (π^*, α, and β parameters) [37–39]. The KT equation relies on a linear solvation energy relationship given by [40]:

$$\mathrm{XYZ} = (\mathrm{XYZ})_0 + \mathrm{s}(\pi^* + \mathrm{d}\delta) + \mathrm{a}\alpha + \mathrm{b}\beta \tag{9}$$

where XYZ is a certain property of the solute (e.g., solubility, equilibrium constant, reaction rate, etc.) in a given solvent, XYZ_0 is the same property in a reference state, π^* is the solvent's dipolarity/polarizability, δ is a polarizability correction term, α and β are measures for the hydrogen-bond donating and hydrogen-bond accepting ability of the solvent. a, b, d and s are constants. Experimental measurements of E_T or KT parameters are time consuming, while a proper probe molecule should be very carefully chosen to avoid solubility and stability problems [41, 42].

DESs are a new class of solvents that can be obtained by mixing a hydrogen bond acceptor (HBA) and a hydrogen bond donor (HBD) in a specific ratio to yield a eutectic mixture, which has a much lower melting point than the two starting materials [43–46]. Compared to ILs, DESs are less toxic, mostly biodegradable, and cheaper, while sharing many of the interesting properties of ILs, such as low volatility, low melting point, good solvation properties, and tunability [47–52]. For these reasons, DESs have been proposed as an environmentally friendly alternative to the currently used volatile organic compounds (VOCs) [53–56]. Due to the large number of possible DESs and limited experimental polarity data, it is not straightforward to select the best candidate for a specific application. In screening studies, it is often sufficient to have a rough estimate of the polarity of a solvent. Hence, molecular simulation can be a powerful tool to estimate the polarity of a solvent by the computation of the dispersion, polar, and hydrogen bonding contributions of the solubility parameter. Molecular simulations have indeed been used to compute the SPs of ionic liquids, organic solvents, pharmaceuticals, and polymers [31, 57–60], as well as to compute a variety of properties and analyze the structure of DESs [61–64]. To the best of our knowledge, Molecular Dynamics (MD) simulations have not been used previously to compute SPs of DESs. Therefore, the aim of this work was to compute SPs of choline chloride-based hydrophilic DESs from MD simulations, investigate the effects of temperature and gas phase composition on the SPs, and establish correlations between SPs and other properties of DESs. Whereas SPs of solvent mixtures are mostly obtained from solubility measurements [65], correlations with other physical properties of the mixture [12, 14], or by using mixing rules [2, 66], here, a thermodynamic approach is employed to computed the SPs of DESs by using Equation (1). The DESs studied in this work are listed in Table 1.

This manuscript is organized as follows. In the next section, the simulation details to compute SPs are outlined. In Section 3, the SP results from the MD simulations at various temperatures and vapor phase compositions are presented and compared with available experimental data and/or correlations. Finally, conclusions with respect to the estimation of SPs of non-volatile solvents like DESs are provided.

2. Simulation Details

2.1. Force Field Parameters

The OPLS [67] force field parameters developed for DESs by Doherty and Acevedo [68] were used for all DESs in this work. For comparison, the parameters by Perkins et al. [62]

based on the Generalized AMBER Force Field (GAFF) [69] were also used for choline chloride urea (ChClU). Both force fields are non-polarizable and include non-bonded Lennard-Jones (LJ) and electrostatic energies as well as bonded terms (bond stretching, bond bending and changes in torsional angles). 1-4 intramolecular interaction energies were scaled according to the AMBER [70] (0.5 for LJ and 0.833 for Coulomb energies) and OPLS (0.5 for both LJ and Coulomb energies) force fields. To take the polarization effects into account, the ionic charges were scaled by 0.8, leading to a better agreement of models with experimental results [62, 68, 71]. The intramolecular exclusion terms between hydrogen and oxygen atoms of hydroxyl groups in ethylene glycol, glycerol, oxalic acid and malonic acid were not considered in the simulations. The omission of these interactions had negligible effects on the density (below 1 % relative difference) and the radial distribution functions (RDFs) of the resulting DESs. These interactions are not expected to affect the solubility parameters significantly, as the effect of non-bonded intramolecular interactions on average cancel out in Equation (1). As suggested by Liu et al. [72], $\epsilon = 0.001\,\mathrm{kcal\,mol^{-1}}$ and $\sigma = 0.1\,\text{Å}$ were set as the LJ parameters for unprotected hydrogen atoms in the hydroxyl groups of DES components to prevent atomic overlaps. Force field parameters of all molecules are listed in the Supporting Information.

The particle-particle particle-mesh (PPPM) method, with a relative error of 1×10^{-5}, was used to compute electrostatic energies. Cut off radii of 12 Å and 40 Å were used for both LJ and short-range electrostatic energies in the condensed and gas phase simulations, respectively. The LJ potential was shifted and in the liquid phase simulations, analytic tail corrections were used [73]. The Lorentz-Berthelot and Jorgensen mixing rules were used to compute the LJ potential between non-identical atoms for the GAFF and OPLS models, respectively. Nosé-Hoover thermostat and barostat [74] were used to keep temperature and pressure constant during simulations. All simulations were performed with LAMMPS package [75] (version 16 Feb. 2016) and initial configurations were generated with PACKMOL [76], unless mentioned otherwise.

2.2. Calculation of SPs

Assuming total vaporization of the liquid phase into vapor, the molar energy of vaporization of the DES, ΔE_{vap}, can be computed from MD simulations according to:

$$\Delta E_{\mathrm{vap}} = N_{\mathrm{A}} \frac{\langle \sum_{i=1}^{n} E_{\mathrm{gas},i} - E_{\mathrm{liq}} \rangle}{n} \tag{10}$$

where N_{A} is the Avogadro's number, $\langle ... \rangle$ denotes an ensemble average, n the number of molecules of the vaporizing entity in the liquid phase, $E_{\mathrm{gas},i}$ the energy of an individual entity in the ideal gas phase and E_{liq} the total energy of the condensed phase simulation. The average internal energy of the liquid phase was computed from three independent simulations using different initial configurations. The condensed phase simulations were performed in the isothermal-isobaric (NPT) ensemble. Depending on the DES and simulation temperature, an equilibration time of between 50 ns and 300 ns was required to bring the system to complete equilibration. After reaching equilibrium, production runs of up to 100 ns were performed to accurately compute the various energy components of the system. 50 HBA ion pairs were

used in the simulations, and the number of HBD molecules was adjusted according to the HBA:HBD molar ratio for each DES. The vaporizing entity of the DES was initially assumed to be a DES cluster (i.e., the HBA and HBD complex with the same molar ratio as in the liquid phase). Therefore, the average internal energy of the ideal gas phase was obtained by performing an NVT simulation on a single isolated DES cluster, at the same temperature as the liquid and multiplying the resulting energy by the number of clusters in the liquid phase, according to the summation in Equation (10). From the final configuration of each liquid phase simulation, three DES clusters were randomly selected as initial configurations for the gas phase simulations and the results were subsequently averaged over all the independent simulations. The box size was set to 200 Å to ensure that the interactions between the cluster and its periodic images are negligible. In gas phase simulations of clusters, the DES components stayed close to each other and the initial clusters remained as clusters during the whole simulation. The clusters were equilibrated for 0.5 ns and averages were computed from a production run of 1 ns. A time step of 1 fs was used to integrate the equations of motion in the condensed phase. For the gas phase simulations, the time step was reduced to 0.1 fs to avoid disintegration of the clusters due to momentary repulsion forces. The Hildebrand solubility parameter was obtained using Equation (1) at various temperatures.

The currently available force fields for DESs, including those used here, do not have an explicit hydrogen bond term, which means that the polar and the hydrogen bond contributions of the Hansen SP cannot be obtained separately. For this reason, the polar and the hydrogen bond contributions were combined into a single electrostatic, δ_{e}, term:

$$\delta_{\mathrm{e}} = \sqrt{\delta_{\mathrm{p}}^2 + \delta_{\mathrm{h}}^2} \tag{11}$$

The Hansen SP can be calculated from the average potential energy of the condensed phase simulation and the energy of individual molecules in the gas phase [31]:

$$\delta_k^2 = \left(\frac{\left\langle \sum_{i=1}^{n} E_i^k - E_{\mathrm{liq}}^k \right\rangle}{\langle V_{\mathrm{box}} \rangle} \right) \tag{12}$$

where k are the Hansen components (k = d for dispersion, and k = (p + h) = e for electrostatic), $\langle ... \rangle$ denotes an ensemble average over time and V_{box} is the volume of the liquid phase simulation box. Unlike the Hildebrand SP, the total Hansen SP does not take into account bonded energy terms and only contains contributions from non-bonded dispersion and electrostatic interactions, therefore, it is expected that these two values will slightly differ [31]. The Hansen SPs were computed from the same condensed phase and ideal gas simulations for computing Hildebrand SPs, where in addition to the total potential energy of the system, the contributions by electrostatic and dispersion forces were also obtained for use in Equation (12).

It is important to note that the nature, i.e. the composition and state (e.g., neutral molecules, ion pairs, HBA:HBD complexes, or clusters) of the vapor phase of hydrophilic DESs, such as the ones in this study, is currently unknown. Shahbaz et al. [77] measured the vapor pressure of five different hydrophilic DESs composed of the salts (HBAs)

choline chloride, N,N-diethylethanolammonium chloride, and methyltriphenylphosphonium bromide, and glycerol and urea as the HBDs. In a recent study by Ravula et al. [78], the vapor pressures of choline chloride urea (ChClU), choline chloride glycerol (ChClG), and choline chloride ethylene glycol (ChClEg) were measured. The vapor pressure of ChClG in the latter study was comparable to the one by Shahbaz et al. [77], however, Ravula et al. [78] measured a higher vapor pressure for ChClU. In Figure 1, experimentally measured vapor pressures of ChClU, ChClG, and ChClEg DESs, as a function of temperature, are compared with the pure HBD components of these DESs (urea, glycerol and ethylene glycol) and the [bmim][Tf2N] ionic liquid. As it can be seen in Figure 1, the vapor pressures of the DESs are rather close to the vapor pressures of the pure HBDs. A consistent relation between the vapor pressure of the DESs and that of the pure HBDs, however, is not observed (Figure 1). This may suggest that the gas phase of these DESs is not entirely composed of the more volatile HBDs. Moreover, it has been shown in several studies that the vapor phase of ionic liquids mainly consists of charge neutral ion pairs with one cation and one anion (and no larger clusters) [22, 79–83]. Therefore, our assumption that the gas phase of DESs consists of isolated clusters of HBD and HBA molecules is reasonable. Recently, Dietz et al. [84] computed the total vapor pressures of six hydrophobic DESs, as well as the partial pressures of individual components in these DES mixtures. It was, however, concluded from the obtained experimental data that the vapor phase of the studied hydrophobic DESs was largely dominated by the most volatile component (as either HBD or HBA in the DES). Dietz et al. [84] also suggested that the larger vapor pressure of the DESs compared to some ILs (as also observed in Figure 1) is due to the ability of DES components to separately evaporate from the mixture, whereas the vaporization in ionic liquids only occurs for ion pairs. Thus, in this work, the vaporization energies of HBD and HBA components in the DES mixture were also computed and compared with the vaporization energy of DES clusters. Based on this analysis, it can be determined whether or not the individual components are more likely to vaporize from the DES liquid mixture, compared to HBA-HBD clusters.

To compute the energy of vaporization for a single DES component (e.g HBD), the energy of the liquid phase was obtained before ($E_{\text{liq}}(n)$) and after ($E_{\text{liq}}(n-1)$) removing one molecule of this component from the liquid mixture. The energy of a single component (HBD or HBA) in the ideal gas phase was also computed ($E_{\text{gas}}(1)$). The molar energy of vaporization was then computed using the following equation:

$$\Delta E_{\text{vap}} = N_{\text{A}} \left\langle E_{\text{liq}}(n-1) + E_{\text{gas}}(1) - E_{\text{liq}}(n) \right\rangle \tag{13}$$

Based on this energy of vaporization, the Hildebrand SP was also computed for both components of the DESs, according to Equation (1). Two kinds of heat of vaporization are typically used for mixtures: integral and differential [85]. The integral heat of vaporization corresponds to the total vaporization of the liquid phase, expressed per mole of the mixture. The differential heat of vaporization, however, corresponds to the vaporization of one mole of the mixture from such amount of liquid that the composition of the liquid phase is not changed. Therefore, the vaporization energy of DES clusters, computed from Equation (10), correlates with the integral heat of vaporization. However, the energy difference computed

from Equation (13) does not describe either of the two heats of vaporization, as it assumes partial vaporization of the mixture, while the liquid phase composition changes.

3. Results and Discussion

3.1. SPs from vaporization energy

The energies (and enthalpies) of vaporization were calculated by fitting Equation (2) to the experimental vapor pressure data by Shahbaz et al. [77] and Ravula et al. [78], which were obtained at elevated temperatures ($45-95\,^{\circ}$C and $40-160\,^{\circ}$C, respectively). The same procedure was carried out for the vapor pressure data of hydrophobic DESs, reported by Dietz et al. [84]. The Clausius-Clapeyron equation (Equation (2)) is derived on the basis of equality of chemical potentials of the vaporizing entity in liquid and vapor phases, when temperature and pressure are changed. It is frequently used for the vapor-liquid phase equilibrium of pure compounds, although it can also be derived for a mixture [86]. The Clausius-Clapeyron equation has been used to relate the total vapor pressure of DES mixtures to temperature [78, 84]. The enthalpy of vaporization computed from the this equation, applied to mixtures, is an average of vaporization enthalpies of mixture components according to the vapor phase composition. The vapor phase composition of the studied DESs is currently unknown. Therefore, the vaporization enthalpy computed from Equation (2) can yield useful insight into the vapor phase composition of the DESs, when compared with simulation results. In this work, the vaporization enthalpies from the experimental data were assumed to be temperature-independent and accurate for lower temperatures. A minimum value of the correlation coefficient (R^2) of 0.9831 in the vapor pressure data fitting, indicated that the vapor pressure-temperature relationship can be well described with Equation (2).

The computed enthalpies of vaporization and Hildebrand SPs as well as the total Hansen SPs, and the individual contributions to the Hansen SPs from MD simulations are presented in Table 2 for various DESs at 298.15 K. The vaporization enthalpies from experimental vapor pressure data are also listed in the table. To the best of our knowledge, no experimental data is available for vapor pressure of pure ChClMa and ChClOa DESs. Thus, for these DESs only the values obtained from the simulations are listed. In addition to the DESs in Table 1, the vaporization enthalpies of N,N-diethylethanolammonium chloride glycerol, N,N-diethylethanolammonium chloride urea and methyltriphenylphosphonium bromide glycerol (all with molar ratios of 1:2) from data of Shahbaz et al. [77] and for hydrophobic DESs from data of Dietz et al. [84] were obtained. These values were within a range of 71 kJ mol^{-1} to 93 kJ mol^{-1}. Note that there is ambiguity about the units of the experimental enthalpies of vaporization as the gas composition is unknown. The enthalpies of vaporization from MD simulations were computed based on the vaporization of DES clusters and thus, have the units of kJ per moles of DES cluster. However, in literature, molar masses and molar volumes of DESs are often implicitly reported based on "1 mole of DES", with a HBA to HBD molar ratio of n_1/n_2, as defined by:

$$1\ [\text{mole DES}] = \frac{n_1}{n_1+n_2}[\text{mole HBA}] + \frac{n_2}{n_1+n_2}[\text{mole HBD}] \tag{14}$$

With this definition, 1 mole of DES cluster (composed of n_1 moles of HBA and n_2 moles of HBD) needs to be considered as:

$$1\ [\text{mole DES cluster}] = (n_1 + n_2)\ [\text{mole DES}] \tag{15}$$

To allow for comparison with experimental molar volumes in literature, the computed molar volumes in Table 2 are reported in units of cm^3 per moles of DES. It can be observed that the enthalpies of vaporization obtained from experimental vapor pressures data for ChClU, ChClG and ChClEg are lower than the ones computed from MD simulations. This could be caused by a different experimental vapor phase composition of DESs, compared to the one assumed in the MD simulations, where only DES clusters constituted the vapor phase. It can be observed that the enthalpy of vaporization obtained from the data of Ravula et al. [78] is comparable to the one from the data of Shahbaz et al. [77] for ChClG, while it is much larger in the case of ChClU. The computed enthalpies of vaporization from MD are larger than the enthalpies of vaporization found in literature for many ionic liquids [11, 17, 22, 87–89]. The computed SPs are also larger than the ones reported for ILs [8, 10, 11, 13, 16, 22, 88], indicating a more polar nature of the DESs compared to most ILs, when the vaporizing entity is assumed to be a DES cluster.

The differences between the computed total Hansen and Hildebrand SPs fall within the uncertainty ranges (0.27-0.57 $MPa^{1/2}$), thus, it is not possible to compare these quantities for each DES. Nevertheless, such differences are expected due to the exclusion of bonded interactions in the Hansen SP formulation [31]. The effects of dipole moments of molecules and the hydrogen bonding between them are lumped into the electrostatic component of the Hansen SP, as the used force fields do not have separate hydrogen bonding terms. While ChClU and ChClOa exhibit a larger contribution of electrostatic forces to the total Hansen SP, compared to dispersion forces, the other considered DESs show the opposite. In the case of ChClU, both OPLS and GAFF force fields result in a larger electrostatics component of Hansen SPs than the dispersion component. This comparison implies a high relative importance of dipole-dipole/hydrogen bonding interactions in ChClU and ChClOa, needed to be overcome for vaporization, while in the other DESs, the dispersion forces play a more important role. The two force fields used for ChClU resulted in only slight differences in the computed Hildebrand and total Hansen SPs. Since the HBA is the same for all the DESs, the differences in the computed SPs can be attributed to the effect of HBDs on the interactions within the DESs. Considering the Hildebrand SP (or the total Hansen SP), it can be observed that the DESs containing HBDs with carboxylic acid functional groups (ChClMa and ChClOa) show the highest polarity, followed by ChClU (with an amide group), ChClG and ChClEg (with alcohol groups). The electrostatic contribution to the Hansen SP, however, indicates a much stronger dipolarity/hydrogen bonding for ChClOa, ChClMa and ChClU compared to the alcohol group containing DESs, ChClG and ChClEg.

Pandey et al. [41] investigated the polarity of DESs using absorbance and fluorescence solvatochromic probes and indeed found high polarities for ChClU, ChClEg, ChClG and ChClMa (all with a molar ratio of 1:2), compared to several common molecular solvents and ionic liquids. Nevertheless, the relative polarities of these DESs with respect to each other

was shown to be strongly dependent on the solvatochromic probe used in the experiments. Therefore, it is not possible to make a definitive comparison between the polarities obtained in the aforementioned work and the SPs computed in the present work. In another study, Pandey and Pandey [90] computed the Kamlet-Taft parameters for ChClU, ChClG and ChClEg. The polarizability/dipolarity parameters (π^*) of the DESs were the following: ChClU > ChClG > ChClEg, in agreement with the relative magnitudes of the Hildebrand (or the total Hansen) SPs of the OPLS-DESs in Table 2. Florindo et al. [91] also investigated the polarity of hydrophobic and hydrophilic DESs, using the betaine dye 33 response and Kamlet-Taft parameters. The polarizability/dipolarity of choline chloride-based DESs was shown to be very high compared to common organic solvents and ILs, in agreement with the calculations in this work. The value of π^* for these DESs was the following: ChClU > ChClG > ChClMa > ChClEg. It was observed in this study that the polarizability/dipolarity of the choline chloride-based DESs was similar to the corresponding ILs, but it was much higher that the hydrophobic DESs, consisting of DL-menthol and tetrabutylammonium chloride HBAs.

3.2. Effect of temperature

Moganty and Baltus [10] showed that the SPs of many ILs are insensitive to temperature. In other studies, only a slight decrease in the solubility parameter of most studied ILs with temperature has been suggested [10, 11, 13, 88]. To investigate the influence of temperature on the Hildebrand SPs of DESs, the SPs were computed from MD simulations at elevated temperatures. The temperature dependence of SPs is presented in Figure 2. Within the uncertainties, represented by error bars, the SPs remain constant with temperature. Nevertheless, the computed average values of SPs for ChClU, ChClG and ChClEg may suggest that the SPs for these DESs decrease slightly with temperature. This decrease in the average SP was caused by an increase in the molar volume of the DES accompanied by a reduction in the energy of vaporization. A similar temperature dependence was observed for the total Hansen SPs and the electrostatic and dispersion parts of the Hansen SPs (not shown here). As a result, the same insensitivity of SPs with temperature reported in literature for ILs is also observed for DESs. Consistently, it has been found that the solubility of several materials in DESs is not very sensitive to temperature [92, 93].

In the study of Pandey and Pandey [90], the Kamlet-Taft dipolarity/polarizability parameter, π^*, was observed to negligibly alter with temperature. Although the molar electronic transition energy of betaine dye (E_T) was shown to decrease with temperature, this decrease was mainly attributed to the rise in the HBD acidity (α) and not to a decrease in dipolarity/polarizability of the DESs. The HBA basicity (β) of the DESs was also found to remain constant with temperature. Using responses of ANS and PRODAN probes, contrary to the response of pyrene, also implied weak temperature dependence of the polarity of DESs. These observations are consistent with the temperature dependence of SPs computed in this work; the polarity of the studied DESs seems to hardly depend on temperature.

3.3. Vapor phase composition

In the calculation of Hildebrand and Hansen SPs, the vaporizing entity of DESs was considered to be a cluster composed of HBD and HBA molecules. However, it is likely that the gas phase is not entirely composed of DES clusters. The vapor pressure and enthalpy of vaporization of a DES mixture are strongly affected by the strength of intermolecular interactions within the liquid mixture. The component that is less "bound" to the system, can more easily escape into the gas phase during the vaporization process. It is important to investigate which component of the DES has a lower vaporization enthalpy and thus, dominates the vapor phase. Therefore, the vaporization enthalpies of HBD and HBA components were separately computed based on Equation (13) and compared with those of the DES clusters, presented in Table 2.

The enthalpies of vaporization for HBD and HBA components are listed in Table 3, along with the ones for DES clusters. Here, the units for enthalpies of vaporization are kJ per number of moles of the vaporizing entity. It can be observed that the computed average enthalpy of vaporization for the HBD molecules is smaller than the one for HBA molecules and DES clusters in all the DESs. This implies that it is more likely for the HBD molecules to break free from the condensed phase into the gas phase and thus, the vapor phase of DESs is more likely dominated by the HBD molecules. The values for the HBD vaporization enthalpies are closer to the experimental enthalpies obtained from the Clausius-Clapeyron equation, as shown in Table 2. This further suggests the vaporization of HBD molecules prior to other components. The MD calculations are consistent with the observations of Dietz et al. [84], where the more volatile components dominated the vapor phase of the studied hydrophobic DESs. Assuming the vapor phase is ideal, the mole fraction of the more volatile component in the vapor phase of those hydrophobic DESs can be computed from the reported total and partial pressure data. The vapor phase mole fraction of the volatile component is obtained between 0.84 and 1, depending on the hydrophobic DES and the temperature. The dominance of the vapor phase by the HBD components could be the reason for the close agreement between the vapor pressures of ChClU, ChClG and ChClEg DESs and the corresponding pure HBD components, as shown in Figure 1. It is interesting that while the vaporization enthalpies of HBD components, computed in this work, are lower than the vaporization enthalpies of most ionic liquids, the vaporization enthalpies of HBA components (composed of the choline chloride ion pair) have a similar magnitude to the vaporization enthalpies of ionic liquids, reported in literature [11, 17, 22, 87, 88].

It can be observed that the OPLS and GAFF force fields result in different average values for the HBD vaporization enthalpy of ChClU, despite an overlap of uncertainty ranges of the enthalpies (ca. 12 and 15 $\mathrm{kJ\,mol^{-1}}$, respectively). By comparing the two values with the experimental enthalpies and based on the assumption of HBD vaporization from the mixture, it is implied that the OPLS force field leads to more accurate values for the HBD vaporization enthalpy. Nevertheless, more accurate results are required to confirm this and experimental data are necessary to establish the vapor phase composition of the studied DESs. The computed vaporization enthalpies of the HBD components, glycerol and ethylene glycol in the DES mixtures are comparable to the vaporization enthalpies of these compounds in pure form. The vaporization enthalpies of the pure compounds are

computed from the vapor pressure data in Figure 1 and are approximately, 81 kJ mol^{-1} and 58 kJ mol^{-1}, for glycerol and ethylene glycol, respectively. This indicates a similar magnitude of intermolecular interactions of these molecules in pure form to the ones in the DES mixture.

The corresponding SPs are also listed in Table 3, for which the molar volume was computed based on the number of moles of the vaporizing component, as deemed more consistent. It can be observed that based on the vaporizing entity, the relative magnitudes of SPs can differ among the DESs; for instance, based the vaporization of HBD components, ChClG has a larger solubility parameter compared to ChClEg, as ethylene glycol seems to be more volatile in the DES mixture. However, the opposite is true if the solubility parameters are compared based on the vaporization of HBAs. The computed solubility parameters in both cases of vaporization of HBD and HBA components are similar to the solubility parameters of ionic liquids [8, 10, 11, 13, 16, 22, 88] and suggest that the studied DESs are polar solvents. Further comparisons of solubility parameters are only possible if the gas phase compositions are available from experiments.

3.4. Relation between SPs and other DES properties

Following the approach of Moganty and Baltus [10] for ILs, the energies of vaporization of OPLS-DESs are plotted in Figure 3 as a function of the activation energies of viscosity to obtain the proportionality constant in Equation (5). In this figure, vaporization energies of DES clusters and HBD components from MD simulations and the vaporization energies obtained from experimental vapor pressure data are used. The activation energies of viscosity were taken from experimental data reported in literature [23, 27, 28, 44, 84, 91, 94–98] and averaged. In the references used for the experimental activation energies of viscosity, both the VFT and Arrhenius modelling approaches have been used.

Although a very strong correlation between the quantities is not observed, the data are concentrated within specific areas of the graph. The vaporization energies of DES clusters are scattered around the line $y = 4.41\,x$. Thus, the value of the constant in Equation (5) is computed as 4.41 for DES clusters, a value close to the one reported in literature for ionic liquids ($c \approx 4.3$). Therefore, the amount of work required for the activated flow process to occur, compared to the work to make a hole of the size of the vaporizing molecule, is similar between the DESs and ILs, if DES clusters were to evaporate. The experimental vaporization energies and the HBD vaporization energies from MD, show much smaller proportionality constants of 1.48 and 1.69, respectively. To construct a more accurate correlation between the two quantities in Figure 3, a larger number of data is required. Similar to the the experimentally derived enthalpies of vaporization, there is ambiguity in the units of the activation energy of viscosity, since it is not clear which of the components in the DES mixture mainly participates in the activated flow process.

To correlate the Hildebrand SPs with the surface tensions of DESs, Equation (3) was used. However, instead of the molar volume, V_m, the molecular volume, $V_\mathrm{mol} = V_\mathrm{m}/N_\mathrm{A}$ (N_A is the Avogadro's number), was used here. The parameter $\gamma V_\mathrm{mol}^{-1/3}$ is referred to as the Gordon parameter (G) [22]. Average experimental densities [23, 27, 94–106] and surface tensions [44, 47, 98, 107, 108] from literature were used to determine the Gordon parameter. No surface tension data were found in literature for ChClOa. The computed CEDs (the

squares of Hildebrand SPs) from MD are plotted as a function of the experimental Gordon parameters for the vaporization of cluster and HBD in various OPLS-DESs in Figure 4. The CED and Gordon parameter were both computed based on 1 mole of the vaporizing component. The CEDs from experimental energies of vaporization were not used in this figure, as the units of this quantity are unclear. It can be observed that the CEDs computed for both the vaporization of HBD components and DES clusters are highly correlated with the Gordon parameter (R^2 values of 0.87 and 0.98, respectively). The linear fit to the cluster vaporization data leads to a value of 13.26 for the constant in Equation (3), which is comparable to the values for ionic liquids in literature [22] ($k \approx 11$). This constant value is computed as 7.54 for the HBD vaporization. Similar to the previous analysis of vaporization energy-viscosity activation energy correlation, more data points are required to establish more precise correlations.

4. Conclusions

Hildebrand and Hansen solubility parameters were computed for five DESs from MD simulations, considering HBD, HBA and DES clusters as the vaporizing entity. Relatively large solubility parameters were obtained, which indicates that the studied DESs are polar solvents. The various components of the Hansen SP were computed for the cluster vaporization. The electrostatic component suggested a stronger dipolarity/hydrogen bonding of the carboxylic acid containing DESs. The relative importance of the electrostatic and dispersion contributions were different for different DESs. For ChClU and ChClOa, the electrostatic contribution was larger, while for the other DESs, the dispersion component played a more important role. The computed SPs were relatively insensitive to the imposed temperature, although some of the average SP values suggested a slight decrease in the SPs with temperature. The enthalpies of vaporization were also computed for HBD, HBA and cluster vaporization. For comparison, experimental enthalpies of vaporization were obtained by fitting vapor pressure data from literature to the Clausius-Clapeyron relation. The vapor phase composition of the studied DESs is currently unknown. The smaller values of the vaporization enthalpies of HBD components strongly suggest (also closer to the experimental enthalpies) that the HBD molecules are more likely to vaporize prior to the other entities in the mixture. The GAFF and OPLS force fields resulted in slightly different average vaporization enthalpies and solubility parameters. The computed SPs of the DESs from cluster vaporization simulations were larger than the SPs of common ILs reported in literature, whereas the SPs computed based on HBD or HBA vaporization were comparable to the SPs of ILs. The vaporization energies of DES clusters and HBD components were correlated with the experimental activation energies of viscosity of the DESs. The data implied ratios $\Delta E_{\text{vap}}/E_{\text{a}}^{\text{vis}}$ of 4.41 and 1.69 between the two quantities, for the vaporization of DES cluster and HBD, respectively. The former value is in agreement with the value reported in literature for ILs (≈ 4.3). The correlation between the cohesive energy density of the DESs and the experimental Gordon parameter suggested ratios of 13.26 and 7.54 between the two, for cluster and HBD vaporization, respectively. The former value is close to the value reported for ILs (≈ 11). Nevertheless, to establish more concrete and accurate correlations, more

data points are necessary. Further comparisons of vaporization enthalpies and SPs are only possible if the vapor phase composition of the DESs is available from experimental work. The promising results in this work demonstrate how powerful MD simulations can be to compute and predict the vapor phase composition, enthalpy of vaporization and the solubility parameters of non-volatile compounds, such as DESs. The rough estimations made for the SPs of the DESs in this work can be useful in screening studies that are based on the polarities and solubilities of these DESs with respect to different solutes.

Acknowledgments

This work was sponsored by NWO Exacte Wetenschappen (Physical Sciences) for the use of supercomputer facilities, with financial support from the Nederlandse Organisatie voor Wetenschappelijk Onderzoek (Netherlands Organisation for Scientific Research, NWO). TJHV acknowledges NWO-CW (Chemical Sciences) for a VICI grant.

Table 1: Nomenclature, hydrogen bond acceptor (HBA) and hydrogen bond donor (HBD) components, molar ratios and average molar masses of the DESs used in this work. The average molar mass for each DES was obtained by using the relation $M_{\text{ave}} = \sum x_i M_i$, where x_i is the mole fraction and M_i the molar mass of each DES component (HBD and HBA).

name	HBA	HBD	abbreviation	HBA:HBD	M_{ave}/g.mol^{-1}
reline	choline chloride	urea	ChClU	1:2	86.57
ethaline	choline chloride	ethylene glycol	ChClEg	1:2	87.91
glyceline	choline chloride	glycerol	ChClG	1:2	107.93
maline	choline chloride	malonic acid	ChClMa	1:1	121.84
oxaline	choline chloride	oxalic acid	ChClOa	1:1	114.83

Table 2: Solubility parameters in $MPa^{1/2}$ computed at 298.15 K from MD simulations. The listed SPs include Hildebrand SPs as well as total Hansen SPs and various contributions (dispersion and electrostatic) to the Hansen SPs. The computed molar volumes and enthalpies of vaporization from MD have units of cm^3 per moles of DES and kJ per moles of DES cluster, respectively. The enthalpies of vaporization obtained from the vapor pressure data of Shahbaz et al. [77] and Ravula et al. [78] are also listed and have units of kJ per moles of the unknown vaporizing component.

DES	force field	V_m	δ_d	δ_e	δ_{Hans}	δ_{Hild}	ΔH_{vap}^{sim}	ΔH_{vap}^{exp} [77]	ΔH_{vap}^{exp} [78]
ChClU	GAFF	71.1	18.5	24.9	31.1	30.5	201	46.9	79.0
ChClU	OPLS	75.2	21.8	23.1	31.8	31.6	228	46.9	79.0
ChClG	OPLS	90.8	24.9	19.3	31.5	31.0	265	67.7	70.9
ChClEg	OPLS	78.2	21.8	19.2	29.1	29.3	204	-	55.8
ChClMa	OPLS	99.0	26.4	24.3	35.9	35.6	253	-	-
ChClOa	OPLS	92.5	22.3	25.9	34.2	33.4	217	-	-

Table 3: Enthalpies of vaporization and the corresponding solubility parameters at 298.15 K computed from MD simulations, compared for various vaporizing entities (DES cluster, HBD and HBA). The units of enthalpies and solubility parameters are kJ per moles of the vaporizing component and $MPa^{1/2}$, respectively. The solubility parameters are computed based on the molar volume of the vaporizing entity in the initial liquid phase.

DES	force field	$\Delta H_{\text{vap}}^{\text{HBD}}$	$\Delta H_{\text{vap}}^{\text{HBA}}$	$\Delta H_{\text{vap}}^{\text{cluster}}$	$\delta_{\text{Hild}}^{\text{HBD}}$	$\delta_{\text{Hild}}^{\text{HBA}}$	$\delta_{\text{Hild}}^{\text{cluster}}$
ChClU	GAFF	107	153	201	31.2	26.6	30.5
ChClU	OPLS	82	165	228	26.5	26.8	31.6
ChClG	OPLS	100	148	265	26.8	23.1	31.0
ChClEg	OPLS	73	175	204	24.5	27.1	29.3

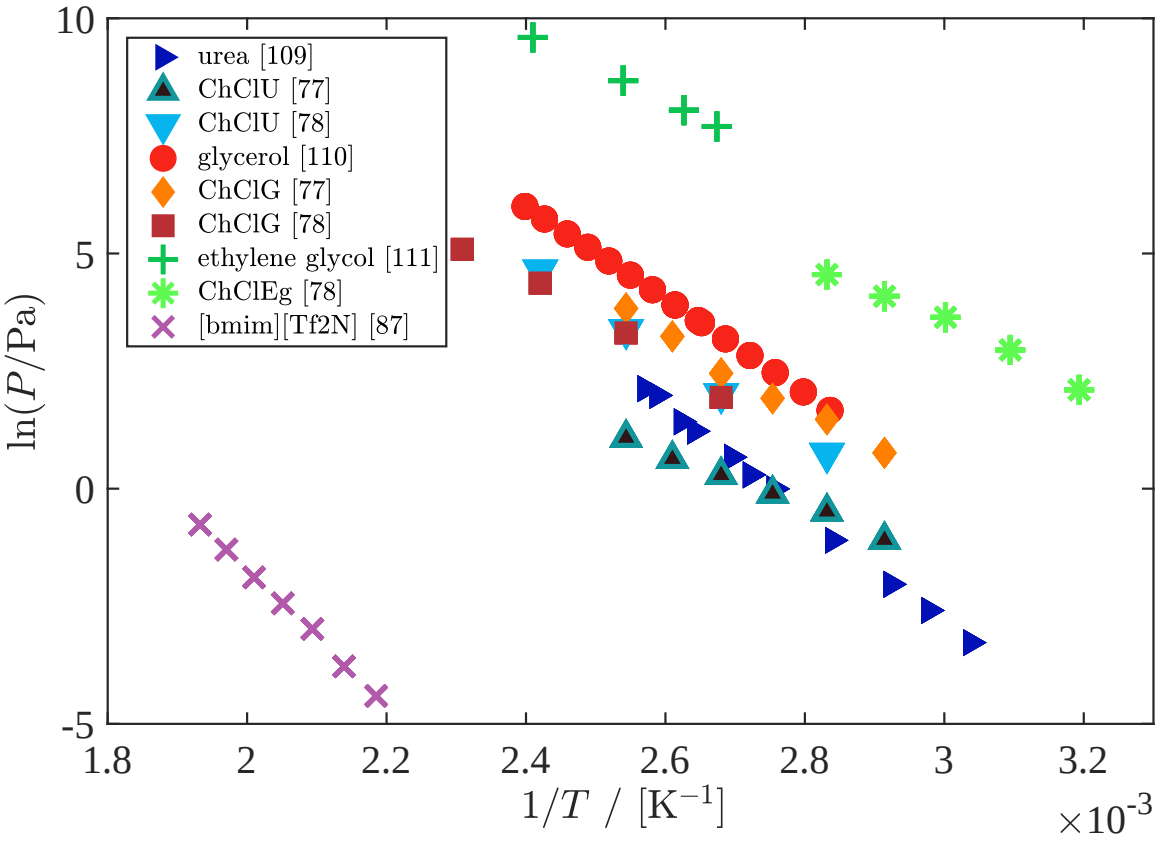

Figure 1: Vapor pressure of the pure HBDs (urea, glycerol and ethylene glycol), the ionic liquid [bmim][Tf_2N], and the choline chloride urea (ChClU), choline chloride glycerol (ChClG), and choline chloride ethylene glycol (ChClEg) deep eutectic solvents with 1:2 molar ratios. The experimental data by Shahbaz et al. [77] and Ravula et al. [78] were used for both ChClU and ChClG. The experimental data by Ravula et al. [78] were also used for ChClEg. The vapor pressure data of pure compounds and the ionic liquid were taken from the experiments of Refs. [87, 109–111].

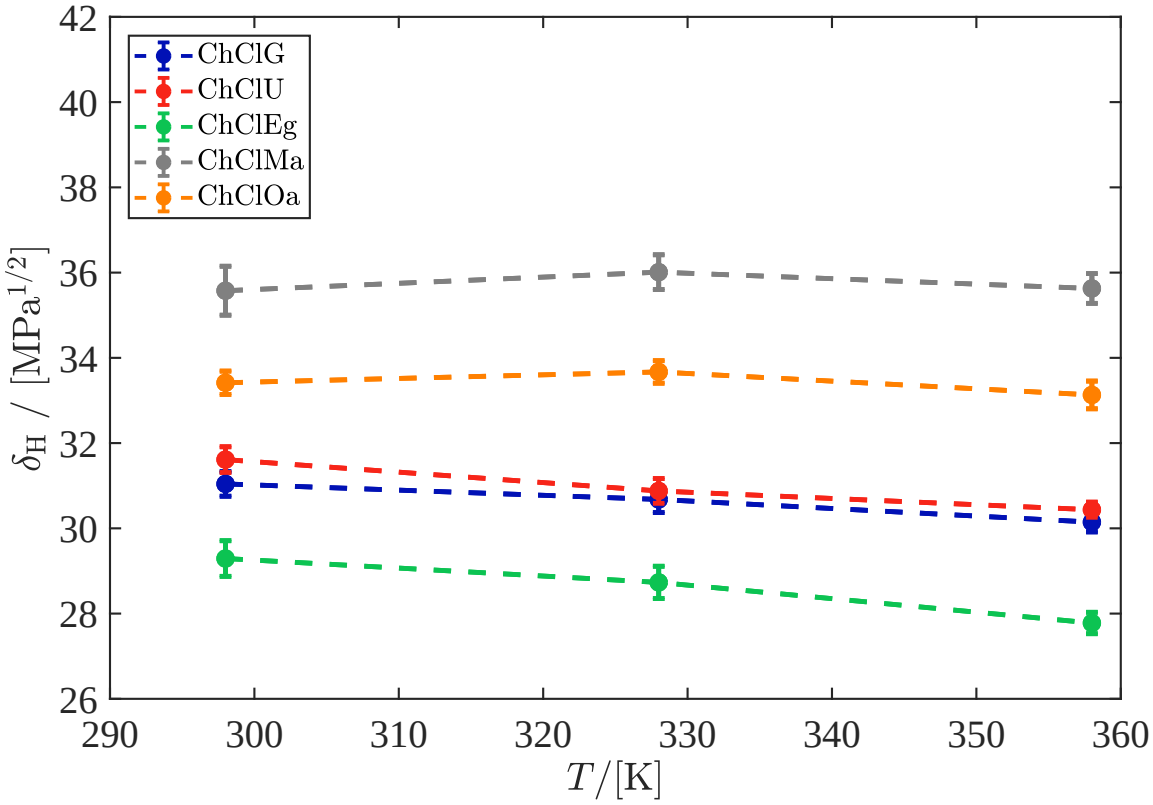

Figure 2: Computed Hildebrand solubility parameters of DESs at different temperatures from MD simulations. The standard deviations are shown with error bars.

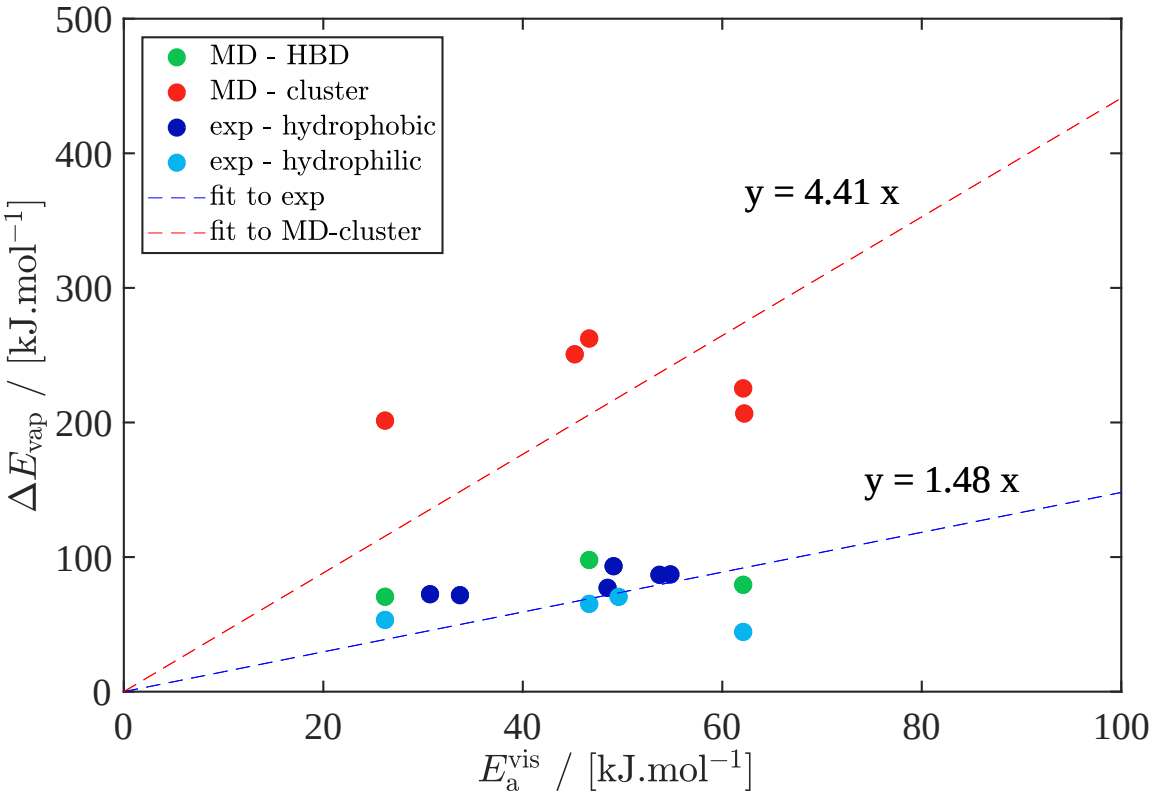

Figure 3: Energy of vaporization of DES clusters (red circles) and HBD components (green circles) from MD simulations and experimental data [77, 78, 84] (light blue for hydrophilic and dark blue for hydrophobic DESs), plotted as a function of the experimental activation energy of viscosity for various DESs. The linear fits to the computed cluster vaporization from MD and the experimental data points are denoted by the red and blue dashed lines, respectively.

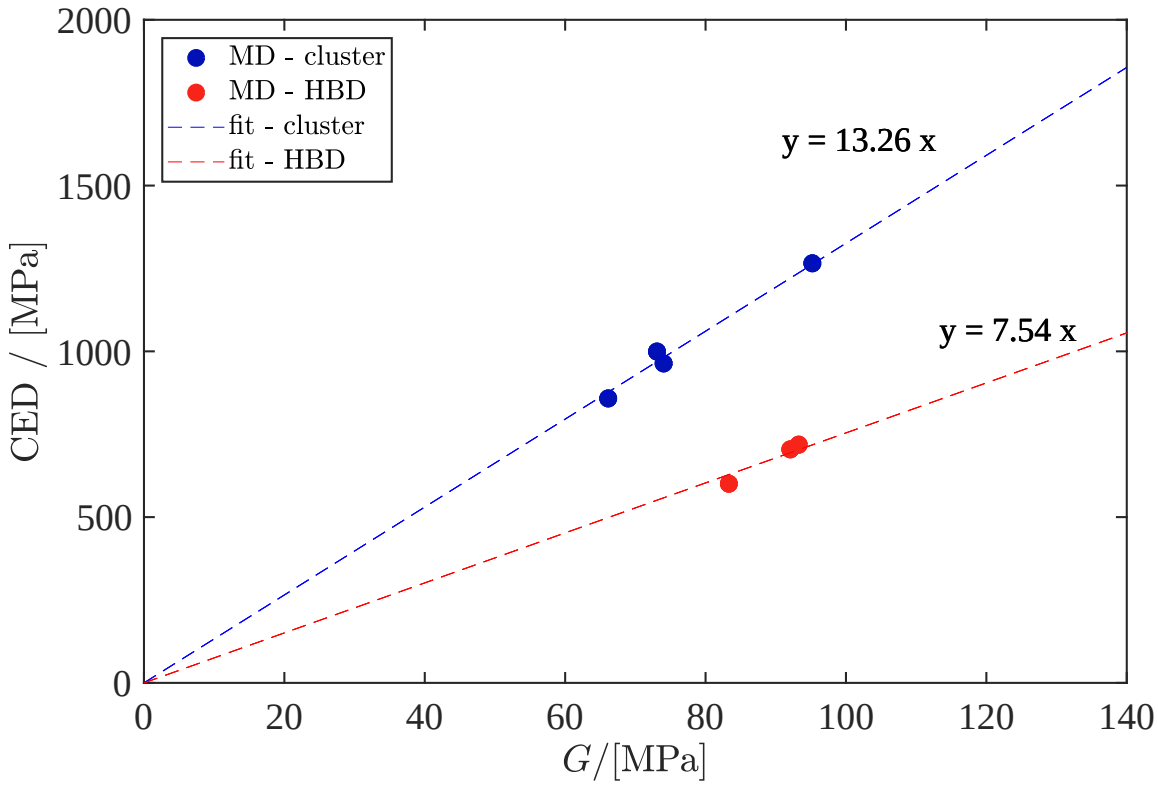

Figure 4: Computed cohesive energy density (CED) from MD simulations, plotted as a function of the experimental Gordon parameter ($\gamma V_{\mathrm{mol}}^{-1/3}$) for various DESs. The symbols denote computed data points and the dashed lines represent the linear fits to the data. DES cluster and HBD vaporization data are shown in blue and red colors, respectively.

References

[1] I. Montes, C. Lai, D. Sanabria, Journal of Chemical Education 80 (2003) 447.
[2] A. F. M. Barton, Chemical Reviews 75 (1975) 731–753.
[3] Hildebrand, Journal of the Society of Chemical Industry 55 (1936) 665–665.
[4] M. J. Moran, H. N. Shapiro, D. D. Boettner, M. B. Bailey, Fundamentals of engineering thermodynamics, John Wiley & Sons, 2010.
[5] P. Becher, Journal of Colloid And Interface Science 38 (1972) 291–293.
[6] P. K. Kilaru, R. A. Condemarin, P. Scovazzo, Industrial & Engineering Chemistry Research 47 (2008) 900–909.
[7] P. K. Kilaru, P. Scovazzo, Industrial and Engineering Chemistry Research 47 (2008) 910–919.
[8] S. H. Lee, S. B. Lee, Chemical Communications (2005) 3469–3471.
[9] T. Lindvig, M. L. Michelsen, G. M. Kontogeorgis, Fluid Phase Equilibria 203 (2002) 247–260.
[10] S. S. Moganty, R. E. Baltus, Industrial and Engineering Chemistry Research 49 (2010) 5846–5853.
[11] P. Weerachanchai, Z. Chen, S. S. J. Leong, M. W. Chang, J. M. Lee, Chemical Engineering Journal 213 (2012) 356–362.
[12] P. Weerachanchai, Y. Wong, K. H. Lim, T. T. Y. Tan, J. M. Lee, ChemPhysChem 15 (2014) 3580–3591.
[13] B. Yoo, W. Afzal, J. M. Prausnitz, Industrial and Engineering Chemistry Research 51 (2012) 9913–9917.
[14] R. F. Fedors, Polymer Engineering & Science 14 (1974) 147–154.
[15] D. M. Koenhen, C. A. Smolders, Journal of Applied Polymer Science 19 (1975) 1163–1179.
[16] A. Marciniak, International Journal of Molecular Sciences 11 (2010) 1973–1990.
[17] A. Marciniak, International Journal of Molecular Sciences 12 (2011) 3553–3575.
[18] E. Stefanis, C. Panayiotou, International Journal of Thermophysics 29 (2008) 568–585.
[19] A. Beerbower, Journal of Colloid And Interface Science 35 (1971) 126–132.
[20] D. Mangaraj, S. K. Bhatnager, S. B. Rath, Makromol. Chem. 67 (1963) 75.
[21] R. H. Ewell, H. Eyring, The Journal of Chemical Physics 5 (1937) 726–736.
[22] K. R. J. Lovelock, Royal Society Open Science 4 (2017) 171223.
[23] A. Yadav, S. Pandey, Journal of Chemical and Engineering Data 59 (2014) 2221–2229.
[24] J. R. Sanders, E. H. Ward, C. L. Hussey, Journal of The Electrochemical Society 133 (1986) 325.
[25] O. O. Okoturo, T. J. VanderNoot, Journal of Electroanalytical Chemistry 568 (2004) 167–181.
[26] M. S. Miran, H. Kinoshita, T. Yasuda, M. A. B. H. Susan, M. Watanabe, Physical Chemistry Chemical Physics 14 (2012) 5178–5186.
[27] K. R. Siongco, R. B. Leron, M. H. Li, Journal of Chemical Thermodynamics 65 (2013) 65–72.
[28] A. R. Harifi-Mood, R. Buchner, Journal of Molecular Liquids 225 (2017) 689–695.
[29] H. Jin, B. O'Hare, J. Dong, S. Arzhantsev, G. A. Baker, J. F. Wishart, A. J. Benesi, M. Maroncelli, Journal of Physical Chemistry B 112 (2008) 81–92.
[30] C. M. Hansen, The Three Dimensional Solubility Parameter and Solvent Diffusion Coefficient and Their Importance in Surface Coating Formulation, Ph.D. thesis, Technical University of Denmark, Copenhagen, 1967.
[31] M. Belmares, M. Blanco, W. A. Goddard, R. B. Ross, G. Caldwell, S. H. Chou, J. Pham, P. M. Olofson, C. Thomas, Journal of Computational Chemistry 25 (2004) 1814–1826.
[32] C. Bordes, V. Fréville, E. Ruffin, P. Marote, J. Y. Gauvrit, S. Briançon, P. Lantéri, International Journal of Pharmaceutics 383 (2010) 236–243.
[33] E. Buncel, S. Rajagopal, Accounts of Chemical Research 23 (1990) 226–231.
[34] S. Nigam, S. Rutan, Applied Spectroscopy 55 (2001) 362A–370A.
[35] C. Reichardt, Chemical Reviews 94 (1994) 2319–2358.
[36] K. Dimroth, C. Reichardt, T. Siepmann, F. Bohlmann, Justus Liebigs Annalen der Chemie 661 (1963) 1–37.
[37] M. J. Kamlet, R. W. Taft, Journal of the American Chemical Society 98 (1976) 377–383.
[38] R. W. Taft, M. J. Kamlet, Journal of the American Chemical Society 98 (1976) 2886–2894.

[39] M. J. Kamlet, J. L. M. Abboud, M. H. Abraham, R. W. Taft, Journal of Organic Chemistry 48 (1983) 2877–2887.
[40] A. R. R. Teles, E. V. Capela, R. S. Carmo, J. A. Coutinho, A. J. Silvestre, M. G. Freire, Fluid Phase Equilibria 448 (2017) 15–21.
[41] A. Pandey, R. Rai, M. Pal, S. Pandey, Physical Chemistry Chemical Physics 16 (2014) 1559–1568.
[42] A. Valvi, J. Dutta, S. Tiwari, Journal of Physical Chemistry B 121 (2017) 11356–11366.
[43] A. P. Abbott, G. Capper, D. L. Davies, R. K. Rasheed, V. Tambyrajah, Chemical Communications (2003) 70–71.
[44] A. P. Abbott, D. Boothby, G. Capper, D. L. Davies, R. K. Rasheed, Journal of the American Chemical Society 126 (2004) 9142–9147.
[45] A. P. Abbott, G. Capper, S. Gray, ChemPhysChem 7 (2006) 803–806.
[46] A. P. Abbott, G. Capper, D. L. Davies, K. J. McKenzie, S. U. Obi, Journal of Chemical and Engineering Data 51 (2006) 1280–1282.
[47] E. L. Smith, A. P. Abbott, K. S. Ryder, Chemical Reviews 114 (2014) 11060–11082.
[48] M. Francisco, A. Van Den Bruinhorst, M. C. Kroon, Angewandte Chemie - International Edition 52 (2013) 3074–3085.
[49] G. García, S. Aparicio, R. Ullah, M. Atilhan, Energy & Fuels 29 (2015) 2616–2644.
[50] D. J. Van Osch, C. H. Dietz, J. Van Spronsen, M. C. Kroon, F. Gallucci, M. Van Sint Annaland, R. Tuinier, ACS Sustainable Chemistry and Engineering 7 (2019) 2933–2942.
[51] L. J. B. M. Kollau, M. Vis, A. van den Bruinhorst, A. C. C. Esteves, R. Tuinier, Chemical Communications 54 (2018) 13351–13354.
[52] L. F. Zubeir, D. J. Van Osch, M. A. Rocha, F. Banat, M. C. Kroon, Journal of Chemical and Engineering Data 63 (2018) 913–919.
[53] A. Paiva, R. Craveiro, I. Aroso, M. Martins, R. L. Reis, A. R. C. Duarte, ACS Sustainable Chemistry & Engineering 2 (2014) 1063–1071.
[54] S. Sarmad, Y. Xie, J. P. Mikkola, X. Ji, New Journal of Chemistry 41 (2016) 290–301.
[55] S. Sarmad, J. P. Mikkola, X. Ji, ChemSusChem 10 (2017) 324–352.
[56] Q. Zhang, K. De Oliveira Vigier, S. Royer, F. Jérôme, Chemical Society Reviews 41 (2012) 7108–7146.
[57] N. Rai, A. J. Wagner, R. B. Ross, J. I. Siepmann, Journal of Chemical Theory and Computation 4 (2008) 136–144.
[58] B. Derecskei, A. Derecskei-Kovacs, Molecular Simulation 34 (2008) 1167–1175.
[59] J. Gupta, C. Nunes, S. Vyas, S. Jonnalagadda, Journal of Physical Chemistry B 115 (2011) 2014–2023.
[60] Y. Luo, R. Wang, W. Wang, L. Zhang, S. Wu, Journal of Physical Chemistry C 121 (2017) 10163–10173.
[61] D. V. Wagle, L. Adhikari, G. A. Baker, Fluid Phase Equilibria 448 (2017) 50–58.
[62] S. L. Perkins, P. Painter, C. M. Colina, Journal of Physical Chemistry B 117 (2013) 10250–10260.
[63] S. Mainberger, M. Kindlein, F. Bezold, E. Elts, M. Minceva, H. Briesen, Molecular Physics 115 (2017) 1309–1321.
[64] S. Kaur, A. Gupta, H. K. Kashyap, Journal of Physical Chemistry B 120 (2016) 6712–6720.
[65] P. Redelius, Energy and Fuels 18 (2004) 1087–1092.
[66] M. J. Chertkoff, A. N. Martin, Journal of the American Pharmaceutical Association 49 (1960) 444–447.
[67] W. L. Jorgensen, D. S. Maxwell, J. Tirado-Rives, Journal of the American Chemical Society 118 (1996) 11225–11236.
[68] B. Doherty, O. Acevedo, The Journal of Physical Chemistry B 122 (2018) 9982–9993.
[69] J. Wang, R. M. Wolf, J. W. Caldwell, P. A. Kollman, D. A. Case, Journal of Computational Chemistry 25 (2004) 1157–1174.
[70] C. I. Bayly, K. M. Merz, D. M. Ferguson, W. D. Cornell, T. Fox, J. W. Caldwell, P. A. Kollman, P. Cieplak, I. R. Gould, D. C. Spellmeyer, Journal of the American Chemical Society 117 (1995) 5179–5197.
[71] H. Liu, E. Maginn, The Journal of Chemical Physics 135 (2011) 124507.
[72] H. Liu, E. Maginn, A. E. Visser, N. J. Bridges, E. B. Fox, Industrial and Engineering Chemistry

Research 51 (2012) 7242–7254.
[73] M. P. Allen, D. J. Tildesley, Computer Simulation of Liquids, Clarendon Press, New York, NY, USA, 1989.
[74] D. Frenkel, B. Smit, Understanding molecular simulation: from algorithms to applications, volume 1, Academic Press, San Diego, California, second edition, 2002.
[75] S. Plimpton, Journal of Computational Physics 117 (1995) 1–19.
[76] L. Martínez, R. Andrade, E. G. Birgin, j. M. Martínez, Journal of Computational Chemistry 30 (2009) 2157–2164.
[77] K. Shahbaz, F. S. Mjalli, G. Vakili-Nezhaad, I. M. AlNashef, A. Asadov, M. M. Farid, Journal of Molecular Liquids 222 (2016) 61–66.
[78] S. Ravula, N. E. Larm, M. A. Mottaleb, M. P. Heitz, G. A. Baker, ChemEngineering 3 (2019) 42.
[79] D. Stresser, F. Goulay, M. S. Kelkar, E. J. Maginn, S. R. Leone, Journal of Physical Chemistry A 111 (2007) 3191–3195.
[80] J. P. Leal, J. M. Esperança, M. E. Da Piedade, J. N. Lopes, L. P. Rebelo, K. R. Seddon, Journal of Physical Chemistry A 111 (2007) 6176–6182.
[81] J. P. Armstrong, C. Hurst, R. G. Jones, P. Licence, K. R. Lovelock, C. J. Satterley, I. J. Villar-Garcia, Physical Chemistry Chemical Physics 9 (2007) 982–990.
[82] V. N. Emel'Yanenko, S. P. Verevkin, A. Heintz, J. A. Corfield, A. Deyko, K. R. Lovelock, P. Licence, R. G. Jones, Journal of Physical Chemistry B 112 (2008) 11734–11742.
[83] S. D. Chambreau, G. L. Vaghjiani, A. To, C. Koh, D. Strasser, O. Kostko, S. R. Leone, Journal of Physical Chemistry B 114 (2010) 1361–1367.
[84] C. H. J. T. Dietz, J. T. Creemers, M. A. Meuleman, C. Held, G. Sadowski, M. van Sint Annaland, F. Gallucci, M. C. Kroon, ACS Sustainable Chemistry & Engineering 7 (2019) 4047–4057.
[85] V. Majer, V. Svoboda, J. Pick, R. Holub, Collection of Czechoslovak Chemical Communications 39 (1974) 11–19.
[86] A. Tamir, Fluid Phase Equilibria 8 (1982) 131–147.
[87] Y. Paulechka, D. H. Zaitsau, G. Kabo, A. Strechan, Thermochimica Acta 439 (2005) 158–160.
[88] Y. Wong, Z. J. Chen, T. T. Y. Tan, J. M. Lee, Industrial and Engineering Chemistry Research 54 (2015) 12150–12155.
[89] W. Guan, N. Chang, L. Yang, X. Bu, J. Wei, Q. Liu, Journal of Chemical and Engineering Data 62 (2017) 2610–2616.
[90] A. Pandey, S. Pandey, Journal of Physical Chemistry B 118 (2014) 14652–14661.
[91] C. Florindo, A. J. McIntosh, T. Welton, L. C. Branco, I. M. Marrucho, Physical Chemistry Chemical Physics 20 (2017) 206–213.
[92] C. H. Dietz, M. C. Kroon, M. Van Sint Annaland, F. Gallucci, Journal of Chemical and Engineering Data 62 (2017) 3633–3641.
[93] F. G. Carin H. J. T. Dietz, Annika Erve, Maaike C. Kroon, Martin van Sint Annaland, C. Held, Fluid Phase Equilibria (2018) 4–7.
[94] O. Ciocirlan, O. Iulian, O. Croitoru, REV. CHIM. (Bucharest) 61 (2010) 721–723.
[95] A. Yadav, S. Trivedi, R. Rai, S. Pandey, Fluid Phase Equilibria 367 (2014) 135–142.
[96] A. Yadav, J. R. Kar, M. Verma, S. Naqvi, S. Pandey, Thermochimica Acta 600 (2015) 95–101.
[97] D. Z. Troter, Z. B. Todorović, D. R. Đokić Stojanović, B. S. Đordević, V. M. Todorović, S. S. Konstantinović, V. B. Veljković, Journal of the Serbian Chemical Society 82 (2017) 1039–1052.
[98] M. K. Alomar, M. Hayyan, M. A. Alsaadi, S. Akib, A. Hayyan, M. A. Hashim, Journal of Molecular Liquids 215 (2016) 98–103.
[99] Y. Xie, H. Dong, S. Zhang, X. Lu, X. Ji, Journal of Chemical and Engineering Data 59 (2014) 3344–3352.
[100] F. Chemat, H. Anjum, A. M. Shariff, P. Kumar, T. Murugesan, Journal of Molecular Liquids 218 (2016) 301–308.
[101] R. B. Leron, M. H. Li, Journal of Chemical Thermodynamics 54 (2012) 293–301.
[102] K. Shahbaz, F. S. Ghareh Bagh, F. S. Mjalli, I. M. AlNashef, M. A. Hashim, Fluid Phase Equilibria

354 (2013) 304–311.
[103] K. Shahbaz, S. Baroutian, F. S. Mjalli, M. A. Hashim, I. M. Alnashef, Thermochimica Acta 527 (2012) 59–66.
[104] K. Shahbaz, F. S. Mjalli, M. A. Hashim, I. M. AlNashef, Fluid Phase Equilibria 319 (2012) 48–54.
[105] R. B. Leron, D. S. H. Wong, M. H. Li, Fluid Phase Equilibria 335 (2012) 32–38.
[106] C. Florindo, F. S. Oliveira, L. P. Rebelo, A. M. Fernandes, I. M. Marrucho, ACS Sustainable Chemistry and Engineering 2 (2014) 2416–2425.
[107] C. D'Agostino, R. C. Harris, A. P. Abbott, L. F. Gladden, M. D. Mantle, Physical Chemistry Chemical Physics 13 (2011) 21383–21391.
[108] F. S. Mjalli, G. Vakili-Nezhaad, K. Shahbaz, I. M. Alnashef, Thermochimica Acta 575 (2014) 40–44.
[109] D. Zaitsau, G. J. Kabo, A. A. Kozyro, V. M. Sevruk, Thermochimica Acta 406 (2003) 17–28.
[110] S. P. Verevkin, D. H. Zaitsau, V. N. Emel'yanenko, A. A. Zhabina, Fluid Phase Equilibria 397 (2015) 87–94.
[111] D. Ambrose, D. J. Hall, The Journal of Chemical Thermodynamics 13 (1981) 61–66.

Supporting information for "Computing solubility parameters of Deep Eutectic Solvents from Molecular Dynamics simulations"

Hirad S. Salehi[a], Mahinder Ramdin[a], Othonas A. Moultos[a], Thijs J.H. Vlugt[a,*]

[a]*Engineering Thermodynamics, Process & Energy Department, Faculty of Mechanical, Maritime and Materials Engineering, Delft University of Technology, Leeghwaterstraat 39, 2628CB Delft, The Netherlands*

In this document, force field parameters used in our MD simulations of deep eutectic solvents (DESs) are presented. Five DESs were used in the simulations: choline chloride urea (ChClU), choline chloride glycerol (ChClG), choline chloride ethylene glycol (ChClEg), choline chloride malonic acid (ChClMa), and choline chloride oxalic acid (ChClOa). For all DESs, the parameters obtained by Doherty and Acevedo [1], based on the OPLS force field [2], were used. Additionally, the Generalized Amber Force Field (GAFF) [3] parameters by Perkins et al. [4] were used for ChClU to investigate the influence of force field on the calculations of solubility parameters and enthalpies of vaporization. Both force fields are non-polarizable and consist of bonded and non-bonded (Lennard-Jones and electrostatic) terms and model the DESs as all-atom, flexible molecules. Molecular structure and atom labels are shown in Figures S1 to S6.

*Corresponding author
Email address: t.j.h.vlugt@tudelft.nl (Thijs J.H. Vlugt)

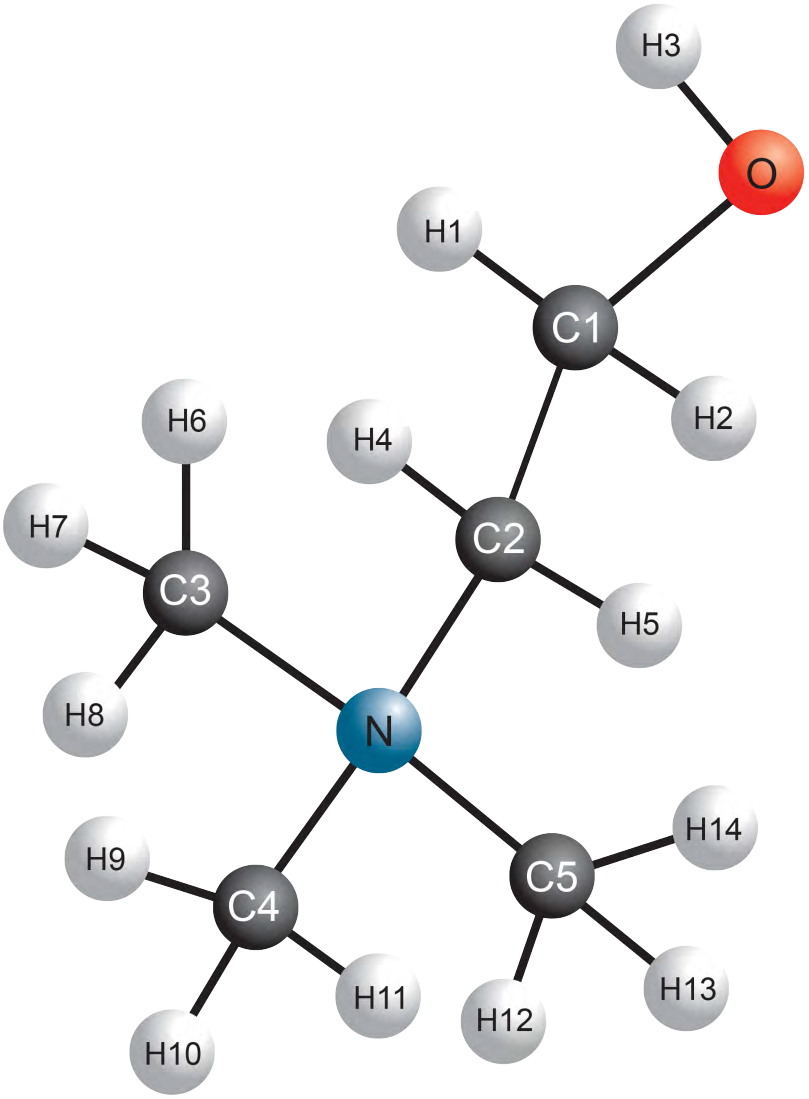

Figure S1: Choline structure and atom labels.

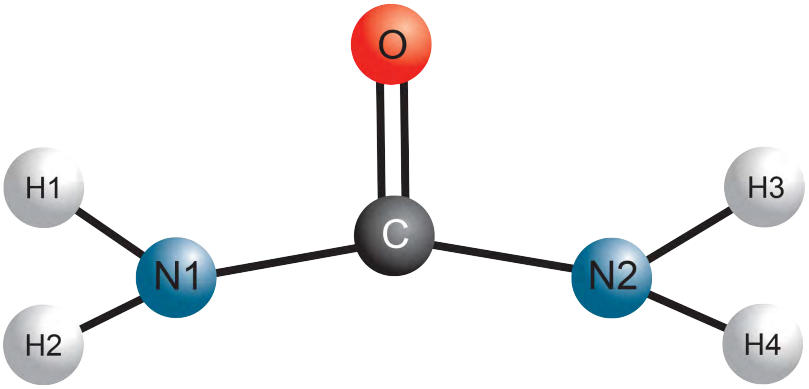

Figure S2: Urea structure and atom labels.

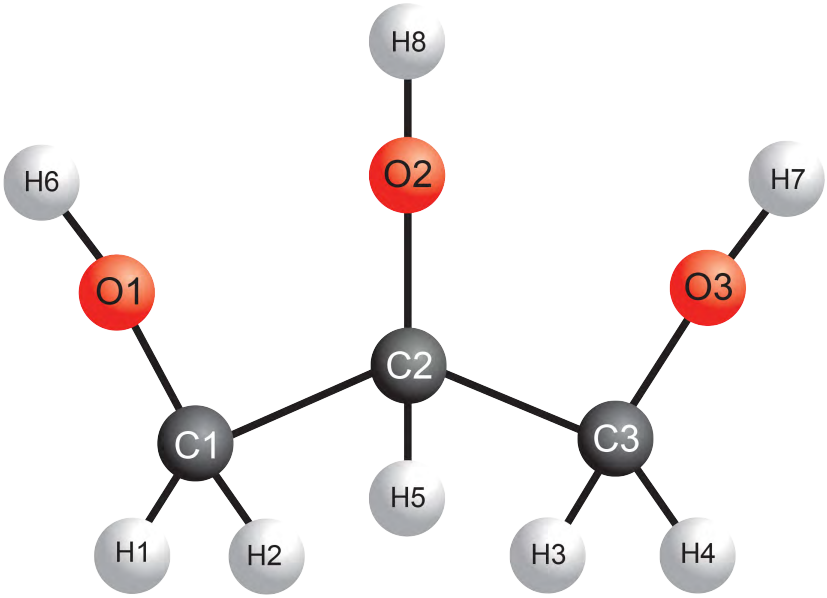

Figure S3: Glycerol structure and atom labels.

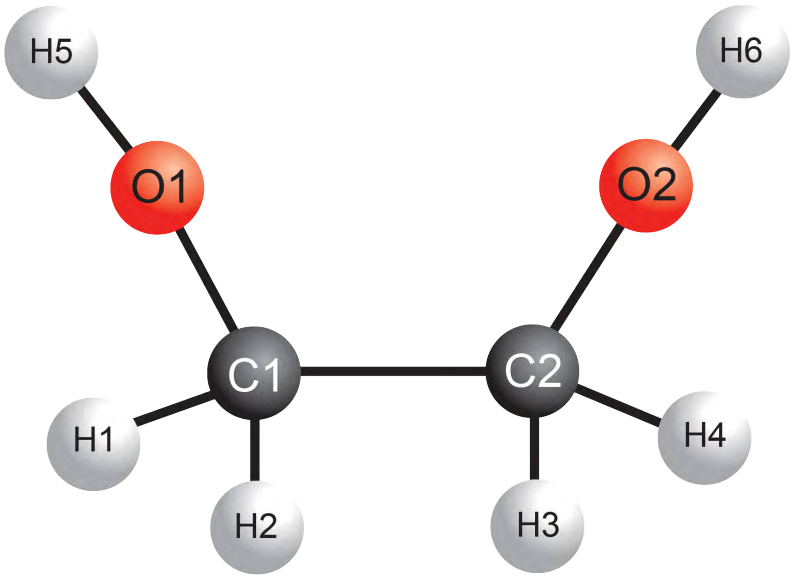

Figure S4: Etyhlene glycol structure and atom labels.

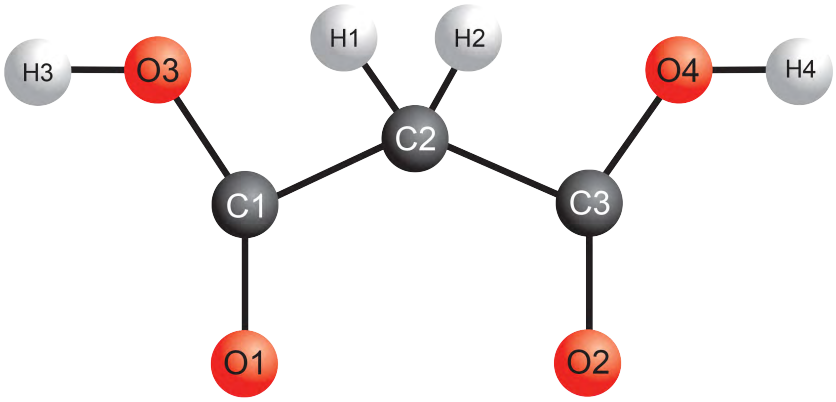

Figure S5: Malonic acid structure and atom labels.

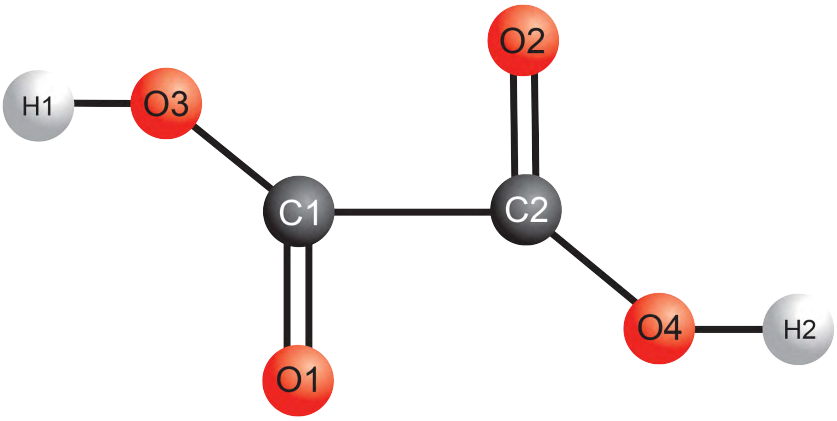

Figure S6: Oxalic acid structure and atom labels.

1. GAFF Force Field Parameters for Choline Chloride

Table S1: GAFF atom types and non-bonded parameters for choline chloride [4].

atom	atom type	partial charge	$\epsilon/(\text{kcal.mol}^{-1})$	$\sigma/(\text{Å})$
C1	CW	0.12008	0.1094	3.3997
C2	CS	-0.02576	0.1094	3.3997
$C3 - C5$	C3	-0.10736	0.1094	3.3997
$H1, H2$	H1	0.04080	0.0157	2.4714
H3	HO	0.36360	0.0010	0.1000
$H4, H5$	HX	0.08928	0.0157	1.9600
$H6 - H14$	HX	0.09544	0.0157	1.9600
N	N4	0.04016	0.1700	3.2500
O	OH	-0.49512	0.2104	3.0665
Cl	Cl	-0.80000	0.1000	4.4010

Table S2: GAFF bond parameters for choline ion [4]. The bond energy is calculated as: $E_{\mathrm{bond}}(r) = k_{\mathrm{r}}(r - r_0)^2$.

bond type	$k_{\mathrm{r}}/(\mathrm{kcal.mol^{-1}.\AA^{-2}})$	$r_0/(\mathrm{\AA})$
C3 − HX	338.7	1.09
C3 − N4	293.6	1.50
N4 − CS	293.6	1.50
CS − HX	338.7	1.09
CS − HX	303.1	1.54
CW − H1	335.9	1.09
CW − OH	314.1	1.43
OH − HO	369.6	0.97

Table S3: GAFF angle parameters for choline ion [4]. The angle energy is calculated as: $E_{\text{angle}}(\theta) = k_\theta(\theta - \theta_0)^2$.

angle type	$k_\theta/(\text{kcal.mol}^{-1}.\text{rad}^{-2})$	θ_0
HX − C3 − HX	39.04	110.7
HX − C3 − N4	49.02	107.9
C3 − N4 − CS	62.84	110.6
N4 − CS − HX	49.02	107.9
N4 − CS − CW	64.45	114.3
CS − CW − H1	46.36	110.1
CS − CW − OH	67.72	109.4
HX − CS − CW	46.02	111.7
H1 − CW − OH	50.97	109.9
CW − OH − HO	47.09	108.2
C3 − N4 − C3	62.84	110.6
HX − C3 − HX	39.04	110.7
H1 − CW − H1	39.18	109.6

Table S4: GAFF dihedral parameters for choline ion [4]. The dihedral energy is calculated as: $E_{\text{dihedral}}(\phi) = \frac{V_n}{2}[1 + \cos(n\phi - \gamma)]$.

dihedral types	$\frac{V_n}{2}/(\text{kcal.mol}^{-1})$	n	γ
$H1 - CW - OH - HO$	0.167	3	0
$CS - CW - OH - HO$	0.160	-3	0
$CS - CW - OH - HO$	0.250	1	0
$H1 - CW - CS - HX$	0.156	3	0
$H1 - CW - CS - N4$	0.156	3	0
$OH - CW - CS - HX$	0.156	3	0
$OH - CW - CS - N4$	0.156	3	0
$CW - CS - N4 - C3$	0.156	3	0
$HX - CS - N4 - C3$	0.156	3	0
$CS - N4 - C3 - HX$	0.156	3	0
$C3 - N4 - C3 - HX$	0.156	3	0

2. GAFF Force Field Parameters for Urea

Table S5: GAFF atom types and non-bonded parameters for urea [4].

atom	atom type	partial charge	$\epsilon/(\text{kcal.mol}^{-1})$	$\sigma/(\text{Å})$
C	C	1.0401	0.0860	3.3997
H1, H3	HZ	0.4167	0.0157	1.0691
H2, H4	HN	0.4167	0.0157	1.0691
N1, N2	N	-1.0246	0.1700	3.2500
O	O	-0.6577	0.2100	2.9599

Table S6: GAFF bond parameters for urea [4].

bond type	$k_{\mathrm{r}}/(\mathrm{kcal.mol^{-1}.\AA^{-2}})$	$r_0/(\mathrm{\AA})$
$\mathrm{C-O}$	648.0	1.21
$\mathrm{C-N}$	478.2	1.35
$\mathrm{N-HN}$	410.2	1.01

Table S7: GAFF angle parameters for urea [4].

angle type	$k_\theta/(\text{kcal.mol}^{-1}.\text{rad}^{-2})$	θ_0
$\text{N}-\text{C}-\text{O}$	75.83	122.0
$\text{C}-\text{N}-\text{HN}$	49.21	118.5
$\text{C}-\text{N}-\text{HZ}$	49.21	118.5
$\text{HN}-\text{N}-\text{HZ}$	39.73	117.9
$\text{N}-\text{C}-\text{N}$	74.80	113.4

Table S8: GAFF dihedral parameters for urea [4].

dihedral types	$\frac{V_n}{2}$/(kcal.mol^{-1})	n	γ
HN − N − C − O	2.5	-2	180
HN − N − C − O	2.0	1	0
HZ − N − C − O	2.5	-2	180
HZ − N − C − O	2.0	1	0
N − C − N − HN	2.5	2	180
N − C − N − HZ	2.5	2	180
N − N − C − O (improper)	10.5	2	180
C − HZ − N − HN (improper)	1.1	2	180

3. OPLS Force Field Parameters for Choline Chloride

Table S9: OPLS atom types and non-bonded parameters for choline chloride [1].

atom	atom type	partial charge	$\epsilon/(\text{kcal.mol}^{-1})$	$\sigma/(\text{Å})$
C1	CW	0.132	0.066	3.50
C2	CS	-0.131	0.066	3.50
C3 − C5	CA	-0.100	0.066	3.50
H1, H2	HW	0.034	0.030	2.20
H3	HY	0.275	0.001	0.10
H4, H5	HS	0.068	0.030	2.60
H6 − H14	HA	0.033	0.030	2.50
N	NA	0.791	0.170	3.25
O	OY	-0.468	0.170	3.07
Cl	Cl	-0.800	0.148	3.77

Table S10: OPLS bond parameters for choline ion [1]. The bond energy is calculated as: $E_{\mathrm{bond}}(r) = k_{\mathrm{r}}(r - r_0)^2$.

bond type	$k_{\mathrm{r}}/(\mathrm{kcal.mol^{-1}\AA^{-2}})$	$r_0/(\mathrm{\AA})$
HA − CA	340	1.0990
CA − NA	490	1.4980
NA − CS	490	1.5160
CS − HS	340	1.0805
CS − CW	317	1.5210
CW − HW	340	1.0850
CW − OY	450	1.3950
OY − HY	553	0.9490

Table S11: OPLS angle parameters for choline ion [1]. The angle energy is calculated as: $E_{\text{angle}}(\theta) = k_\theta(\theta - \theta_0)^2$.

angle type	k_θ/(kcal.mol^{-1}.rad^{-2})	θ_0
HA − CA − HA	35.0	110.01
HA − CA − NA	35.0	108.90
CA − NA − CS	51.8	110.20
NA − CS − HS	35.0	106.40
NA − CS − CW	70.0	116.60
CS − CW − HW	35.0	108.30
CS − CW − OY	80.0	109.60
HS − CS − CW	35.0	109.30
HW − CW − OY	35.0	111.60
CW − OY − HY	35.0	110.90
CA − NA − CA	55.0	108.73
HS − CS − HS	35.0	108.60
HW − CW − HW	35.0	107.40

Table S12: OPLS dihedral parameters for choline ion [1]. The dihedral energy is calculated as: $E_{\text{dihedral}}(\phi) = \frac{1}{2}V_1[1 + \cos(\phi)] + \frac{1}{2}V_2[1 - \cos(2\phi)] + \frac{1}{2}V_3[1 + \cos(3\phi)]$.

dihedral types	$V_1/(\text{kcal.mol}^{-1})$	$V_2/(\text{kcal.mol}^{-1})$	$V_3/(\text{kcal.mol}^{-1})$
CW − CS − NA − CA	0.100	0.550	0.650
CA − NA − CA − HA	0.000	0.000	0.825
CS − NA − CA − HA	0.000	0.000	0.940
HS − CS − NA − CA	0.000	1.000	0.700
OY − CW − CS − NA	-6.000	-5.000	3.200
OY − CW − CS − HS	-0.500	-2.500	0.250
HW − CW − CS − NA	-6.000	-7.000	0.750
HW − CW − CS − HS	6.000	-3.000	2.000
HY − OY − CW − CS	-0.356	-0.174	0.350
HY − OY − CW − HW	-3.000	1.000	-2.000
CS − NA − CA − CA (improper)	0.000	2.000	0.000
CA − NA − CA − CA (improper)	0.000	2.000	0.000

4. OPLS Force Field Parameters for Urea

Table S13: OPLS atom types and non-bonded parameters for urea [1].

atom	atom type	partial charge	$\epsilon/(\text{kcal.mol}^{-1})$	$\sigma/(\text{Å})$
C	C	0.124	0.1575	3.75
H1, H3	HC	0.276	0.0010	0.10
H2, H4	HT	0.276	0.0010	0.10
N1, N2	N	-0.453	0.2550	3.55
O	O	-0.322	0.3150	2.96

Table S14: OPLS bond parameters for urea [1].

bond type	$k_\mathrm{r}/(\mathrm{kcal.mol^{-1}.\AA^{-2}})$	$r_0/(\mathrm{\AA})$
$\mathrm{O-C}$	570	1.229
$\mathrm{N-C}$	490	1.335
$\mathrm{HT-N}$	434	1.010
$\mathrm{HC-N}$	434	1.010

Table S15: OPLS angle parameters for urea [1].

angle type	$k_\theta/(\text{kcal.mol}^{-1}.\text{rad}^{-2})$	θ_0
O − C − N	80	122.9
C − N − HC	35	119.8
C − N − HT	35	119.8
N − C − N	70	114.2
HC − N − HT	35	120.0

Table S16: OPLS dihedral parameters for urea [1].

dihedral types	$V_1/(\text{kcal.mol}^{-1})$	$V_2/(\text{kcal.mol}^{-1})$	$V_3/(\text{kcal.mol}^{-1})$
HT − N − C − O	0.000	4.900	0.000
HC − N − C − O	0.000	4.900	0.000
HT − N − C − N	0.000	4.900	0.000
HC − N − C − N	0.000	4.900	0.000
HT − N − C − HC (improper)	0.000	21.000	0.000
O − C − N − N (improper)	0.000	5.000	0.000

5. OPLS Force Field Parameters for Glycerol

Table S17: OPLS atom types and non-bonded parameters for glycerol [1].

atom	atom type	partial charge	$\epsilon/(\text{kcal.mol}^{-1})$	$\sigma/(\text{Å})$
C1, C3	CB	0.16000	0.1452	3.50
C2	CM	0.14200	0.1452	3.50
H1 − H4	HC	0.06370	0.0660	2.50
H5	HZ	0.02210	0.0660	2.50
H6, H7	HO	0.03043	0.0010	0.10
H8	HM	0.29120	0.0010	0.10
O1, O3	OH	-0.54700	0.3740	3.07
O2	OM	-0.54470	0.3740	3.07

Table S18: OPLS bond parameters for glycerol [1].

bond type	$k_\mathrm{r}/(\mathrm{kcal.mol^{-1}.\AA^{-2}})$	$r_0/(\mathrm{\AA})$
OM − CM	320	1.410
CB − CM	268	1.529
HM − OM	553	0.945
HZ − CM	340	1.090
HC − CB	340	1.090
OH − CB	320	1.410
HO − OH	553	0.945

Table S19: OPLS angle parameters for glycerol [1].

angle type	$k_\theta/(\text{kcal.mol}^{-1}.\text{rad}^{-2})$	θ_0
OM − CM − CB	50.00	108.5
CM − OM − HM	55.00	108.5
OM − CM − HZ	35.00	109.5
CM − CB − HC	37.50	110.7
CM − CB − OH	50.00	109.5
CB − OH − HO	55.00	108.5
CB − CM − CB	58.35	112.7
CB − CM − HZ	37.50	110.7
HC − CB − HC	33.00	107.8
HC − CB − OH	35.00	109.5

Table S20: OPLS dihedral parameters for glycerol [1].

dihedral types	V_1/(kcal.mol^{-1})	V_2/(kcal.mol^{-1})	V_3/(kcal.mol^{-1})
HM − OM − CM − CB	-0.356	-0.174	0.492
HZ − CM − OM − HM	0.000	0.000	0.352
HC − CB − CM − OM	0.000	0.000	0.468
OH − CB − CM − OM	12.234	0.000	0.000
HO − OH − CB − CM	-0.356	-0.174	0.492
HC − CB − CM − CB	0.000	0.000	0.300
OH − CB − CM − CB	-1.552	0.000	0.000
HC − CB − CM − HZ	0.000	0.000	0.300
OH − CB − CM − HZ	0.000	0.000	0.468
HO − OH − CB − HC	0.000	0.000	0.352

6. OPLS Force Field Parameters for Ethylene Glycol

Table S21: OPLS atom types and non-bonded parameters for ethylene glycol [1].

atom	atom type	partial charge	$\epsilon/(\text{kcal.mol}^{-1})$	$\sigma/(\text{Å})$
C1, C2	CG	0.116	0.1155	3.50
H1 − H4	HG	0.048	0.0525	2.50
H5, H6	HO	0.348	0.0010	0.10
O1, O2	OG	-0.560	0.2975	3.00

Table S22: OPLS bond parameters for ethylene glycol [1].

bond type	$k_\mathrm{r}/(\mathrm{kcal.mol^{-1}.\AA^{-2}})$	$r_0/(\mathrm{\AA})$
OG − HO	553	0.945
CG − OG	320	1.410
CG − CG	268	1.529
HG − CG	340	1.090

Table S23: OPLS angle parameters for ethylene glycol [1].

angle type	$k_\theta/(\text{kcal.mol}^{-1}.\text{rad}^{-2})$	θ_0
HO − OG − CG	55.0	108.5
OG − CG − CG	50.0	108.0
OG − CG − HG	35.0	109.5
CG − CG − HG	37.5	110.7
HG − CG − HG	33.0	107.8

Table S24: OPLS dihedral parameters for ethylene glycol [1].

dihedral types	V_1/(kcal.mol^{-1})	V_2/(kcal.mol^{-1})	V_3/(kcal.mol^{-1})
OH − CG − CG − OH	3.887	-1.192	3.206
CG − CG − OH − HO	0.413	-0.754	1.028

7. OPLS Force Field Parameters for Malonic Acid

Table S25: OPLS atom types and non-bonded parameters for malonic acid [1].

atom	atom type	partial charge	$\epsilon/(\text{kcal.mol}^{-1})$	$\sigma/(\text{Å})$
C1, C3	CD	0.416	0.2625	3.75
C2	CT	-0.096	0.1650	3.50
H1, H2	HC	0.048	0.0750	2.50
H3, H4	HO	0.360	0.0010	0.10
O1, O2	OD	-0.352	0.5250	2.96
O3, O4	OH	-0.424	0.4250	3.00

Table S26: OPLS bond parameters for malonic acid [1].

bond type	$k_\mathrm{r}/(\mathrm{kcal.mol^{-1}.\AA^{-2}})$	$r_0/(\mathrm{\AA})$
OD − CD	570	1.229
OH − CD	450	1.364
CT − CD	317	1.522
HO − OH	553	0.945
HC − CT	340	1.090

Table S27: OPLS angle parameters for malonic acid [1].

angle type	$k_\theta/(\text{kcal.mol}^{-1}.\text{rad}^{-2})$	θ_0
OD − CD − OH	80	121.0
OD − CD − CT	80	120.4
CD − OH − HO	35	113.0
CD − CT − CD	63	111.1
CD − CT − HC	35	109.5
CT − CD − OH	70	108.0
HC − CT − HC	33	107.8

Table S28: OPLS dihedral parameters for malonic acid [1].

dihedral types	$V_1/(\text{kcal.mol}^{-1})$	$V_2/(\text{kcal.mol}^{-1})$	$V_3/(\text{kcal.mol}^{-1})$
HO − OH − CD − CT	1.500	5.500	0.000
HC − CT − CD − OD	0.000	0.000	0.000
CD − CT − CD − OH	1.000	0.546	0.450
HC − CT − CD − OH	0.000	0.000	0.000
OD − CD − OH − HO	0.000	5.500	0.000
OD − CD − CT − CD	0.000	0.000	0.000
OH − CD − OD − CT (improper)	0.000	21.000	0.000

8. OPLS Force Field Parameters for Oxalic acid

Table S29: OPLS atom types and non-bonded parameters for oxalic acid [1].

atom	atom type	partial charge	$\epsilon/(\text{kcal.mol}^{-1})$	$\sigma/(\text{Å})$
C1, C2	CD	0.416	0.1575	3.75
H1, H2	HO	0.330	0.0010	0.10
O1, O2	OD	-0.352	0.3150	2.96
O3, O4	OH	-0.394	0.2550	2.92

Table S30: OPLS bond parameters for oxalic acid [1].

bond type	$k_{\mathrm{r}}/(\mathrm{kcal.mol^{-1}.\AA^{-2}})$	$r_0/(\mathrm{\AA})$
OD − CD	570	1.229
OH − CD	450	1.364
CD − CD	350	1.510
HO − OH	553	0.945

Table S31: OPLS angle parameters for oxalic acid [1].

angle type	$k_\theta/(\text{kcal.mol}^{-1}.\text{rad}^{-2})$	θ_0
$\text{OH}-\text{CD}-\text{OD}$	80.00	121.00
$\text{CD}-\text{OH}-\text{HO}$	35.00	113.00
$\text{CD}-\text{CD}-\text{OH}$	70.96	118.03
$\text{CD}-\text{CD}-\text{OD}$	80.00	121.40

Table S32: OPLS dihedral parameters for oxalic acid [1].

dihedral types	V_1/(kcal.mol^{-1})	V_2/(kcal.mol^{-1})	V_3/(kcal.mol^{-1})
HO − OH − CD − CD	3.000	5.500	0.000
OH − CD − CD − OH	1.600	3.200	0.000
HO − OH − CD − OD	0.000	5.500	0.000
OD − CD − CD − OH	1.600	3.200	0.000
OD − CD − CD − OD	1.600	3.200	0.000
OH − CD − OD − CD (improper)	0.000	21.000	0.000

References

[1] B. Doherty, O. Acevedo, The Journal of Physical Chemistry B 122 (2018) 9982–9993.

[2] W. L. Jorgensen, D. S. Maxwell, J. Tirado-Rives, Journal of the American Chemical Society 118 (1996) 11225–11236.

[3] J. Wang, R. M. Wolf, J. W. Caldwell, P. A. Kollman, D. A. Case, Journal of Computational Chemistry 25 (2004) 1157–1174.

[4] S. L. Perkins, P. Painter, C. M. Colina, Journal of Physical Chemistry B 117 (2013) 10250–10260.